Turbulence and internal waves in side-heated convection

Andrew Belmonte,* Andreas Tilgner,† and Albert Libchaber‡
Department of Physics, Joseph Henry Laboratories, Princeton University, Princeton, New Jersey 08544
(Received 1 August 1994)

We present an experimental study of the convective motion of gas contained in a cubic cell heated from the side. The Rayleigh number (Ra) is varied from 4×10^5 to 1×10^{11} by changing the pressure of the gas. Using local temperature probes and shadowgraph visualization, we observe two distinct types of motion coexistent in the cell: turbulent flow and waves. A turbulent large scale circulation around the periphery of the cell, with side eddies along each plate, is observed for $\mathrm{Ra}>3\times10^7$. The turbulent fluctuations are confined to the regions near the hot and cold plates, while the bulk of the cell is stably stratified. We measure the thermal boundary layer thickness; its scaling with Ra has an exponent close to $\frac{2}{7}$, as measured in Rayleigh-Bénard convection. In the central part of the cell, we observe internal waves, with a frequency corresponding to the Brunt-Väisälä frequency of the mean vertical temperature gradient. This system provides a laboratory environment for the study of fluctuation-generated gravitational waves in stratified gases.

PACS number(s): 47.27.−i, 92.60.Ek, 92.60.Dj

I. INTRODUCTION

Among turbulent flows, thermally driven turbulence has in recent years received particular attention. The convective motion occurs in a well-defined system for which the most important control parameter, the Rayleigh number (Ra), can be varied over many decades. The turbulent states can be conveniently characterized by accurate temperature measurements performed with small probes. Rayleigh-Bénard convection (meaning a cell geometry with a vertical temperature gradient imposed by the upper and lower boundaries) has been studied in great detail in cells of different aspect ratios filled with all fluids available in the laboratory. Particularly in gases, with a Prandtl number (Pr) equal to 0.7, the Rayleigh number dependence can be conveniently explored since it is possible to vary Ra over many decades using low temperature helium [1], or room temperature gas [2]. In a cylindrical cell of helium at 5 K, $\mathrm{Ra}\sim10^{14}$ has been reached under Boussinesq conditions.

This paper presents a study of convection driven by a *horizontal* temperature gradient. We investigate convection in a cube filled with gas under pressure, with two facing vertical plates held at different temperatures. The Rayleigh number is varied form 10^5 to 10^{11} by changing the pressure (0.5 to 20 atm) and the gas (He, N_2, or SF_6). The flow in the cell is turbulent along the perimeter, with the strongest activity at the cold and hot plates. Surprisingly, the dependence of the thermal boundary layer thickness on Ra is the same as the hard turbulent state in the Rayleigh-Bénard flow. The center region is stably stratified, and internal (gravitational) waves are observed.

II. BACKGROUND AND EXPERIMENTAL APPARATUS

The investigation of side-heated convection has been largely confined to vertical slots, i.e., cells of large aspect ratio [3]. An excellent systematic study of laminar and turbulent flow in side-heated convection was performed by Elder using water and oil [4,5]. Studies of square cavities have been rare, although important observations were made by Elder in his silicone oil experiment. He observed a circulating laminar flow in the cell with fluid rising in the vicinity of the hot wall and falling along the opposite, cold side. Two recirculations or eddies also developed along the hot and cold sidewalls (see Fig. 8 of [4]), defining two compressed rolls. If L is the separation of the thermally regulated vertical plates, then the characteristic extension of these rolls was $0.09L$ from the sidewalls (for $\mathrm{Ra}=9.6\times10^6$); their height was about L. No motion was detected in the central region of the cell.

Such a side-heated cavity is essentially a Rayleigh-Bénard convection cell rotated by 90° around a horizontal axis. The experimental setup we used is the same as the one previously employed for a study of Rayleigh-Bénard convection; a detailed description is given elsewhere [2,6], so only the gross features are repeated here. A steel high pressure vessel [Fig. 1(a)] contained a cubic convection cell of height L (either 15 or 17 cm). One vertical wall, of brass, was electrically heated while the opposing wall, also of brass, was thermally regulated by a water bath. Thus the boundary conditions at these two walls are isothermal. The other four walls of the cell were plexiglas, and were not temperature controlled. They were howev-

*Present address: Institut Non-Linéaire de Nice, 1361 route des Lucioles, 06560 Valbonne, France (address to which correspondence should be sent).
†Present address: Physikalisches Institut, Universität Bayreuth, 95440 Bayreuth, Germany.
‡Also at NEC Research Institute, 4 Independence Way, Princeton, NJ 08540.

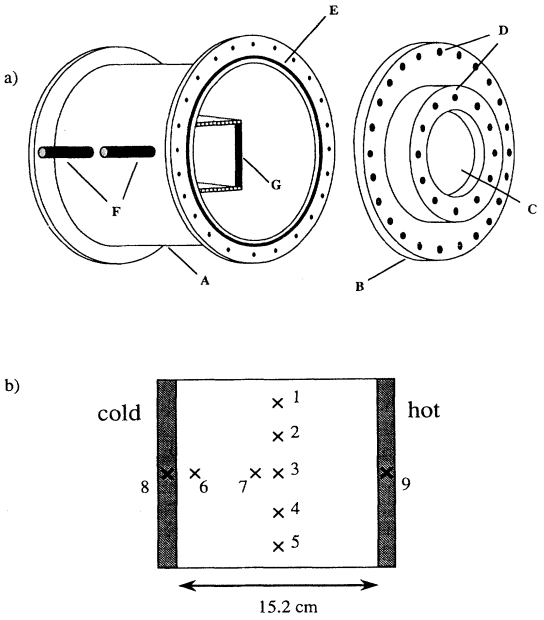

FIG. 1. (a) A diagram of the pressure vessel (A), endcap (B), 2 in. thick plexiglas window (C), bolts (D), o-ring (E), water pipes (F), and convection cell with hot plate visible (G). (b) A schematic diagram of the cell used for local temperature measurements in side-heated convection ($L=15.2$ cm). Temperature probes are located: along a vertical line through the center of the cell (1–5), on a horizontal movable support near the center of the cold plate (6,7), and in the cold and hot plates (8,9).

er insulated on the outside to minimize the heat flux through them [2].

We varied Ra by varying the density of the gas in the cell; this was accomplished by changing the pressure, and by using different gases. The cell was filled with either He, N_2, or SF_6 at pressures from 0.5 to 20 atm. A small hole in the convection cell allowed pressure inside to equilibrate with the rest of the pressure vessel. The temperature difference applied to the cell ranged from 10 to 30 °C. With these parameters, Ra was varied from 10^5 to 10^{11} using the same cell, while $Pr=0.7$.

The basic geometry of the convection cell is shown in Fig. 1(b). Two types of measurements were performed in our experiments: a shadowgraph visualization of the boundary layer region, and local temperature measurements with movable temperature probes.

III. MEASUREMENTS: VISUALIZATION

A complete description of the visualization is to be found elsewhere [6]. We used a cubic experimental cell with $L=17.0$ cm. To visualize the turbulent flow, we used the standard shadowgraph technique [7], in which a parallel beam of light passing through the fluid is focused or defocused by differences in the index of refraction. In our case these differences come from temperature fluctuations in the gas; the intensity variations seen in the shadowgraph image are caused by the second spatial derivative of the temperature. For our purposes the shadowgraph is a convenient way to follow thermal objects in the flow.

Our optical setup consisted of two main parts. The illuminator provided a collimated beam of light which passed through the cell. On the other side of the cell, the imaging system projected the shadowgraph image onto a charge-coupled-device camera, and each image was computer processed. The essential aspect of our image processing system is background subtraction. Working with gas under pressure required that the plexiglas windows of the pressure vessel be 2 in. thick. These windows are the main source of "noise" in the shadowgraph images. Because this noise does not change with time, a long enough time average of the images contains only the noise (the background); the structures in the flow will average out. To "background subtract" our images, were first make a time average and store it in the memory of the video processing hardware in our computer. This hardware then allows us to subtract this averaged image in real time from the incoming video images of the flow. The resulting image reveals structures in the flow with greatly improved clarity. Finally, we adjust the contrast and gray level of the image before recording it onto video tape. Our image capturing, manipulation, and background subtraction was done using a Macintosh computer [8].

We first took video images of the whole cell, but they are not good enough for reproduction, so to indicate the scale of the motion we sketch the observed turbulent flow in Fig. 2(a). A large scale flow and a compressed roll along the hot plate was observed, and no motion or activity in the center region of the cell. The fluid rose along the hot plate, defining an apparent turbulent region which grew with height (as sketched). This region increased dramatically in size and activity along the upper half of the plate. When it reached the corner, the hot fluid divided into two flow directions, one along the horizontal top wall, and the other returning downward parallel to the hot plate. This recirculating eddy is similar to the one observed by Elder [4].

The insets of Fig. 2 show the time development of two perturbations along the hot plate. In Fig. 2(b), a burst of hot fluid moves horizontally away from the plate, and at the same time is advected upwards by the large scale flow. Figure 2(c) shows a similar burst, and above it the development of the turbulent region in the upper half of the cell. Those bursts of activity are intermittent; most of the time the flow is confined near the plate, as shown in the rest of Figs. 2(b) and 2(c). This general description of the flows in the cell is valid from Ra from 3×10^7 to 1×10^{11}, the turbulent regime.

IV. MEASUREMENTS: LOCAL TEMPERATURE

We measured the local temperature in the cell with thermistors, about 200 μm in size, placed throughout the cell ($L=15.2$ cm) as shown in Fig. 1(b). Five thermistors were arranged at fixed positions on a vertical line running through the center of the cell (one in the exact center) to measure the vertical temperature gradient. Several probes were moved on a horizontal line, from the center of the cold plate to the center of the cell, using a

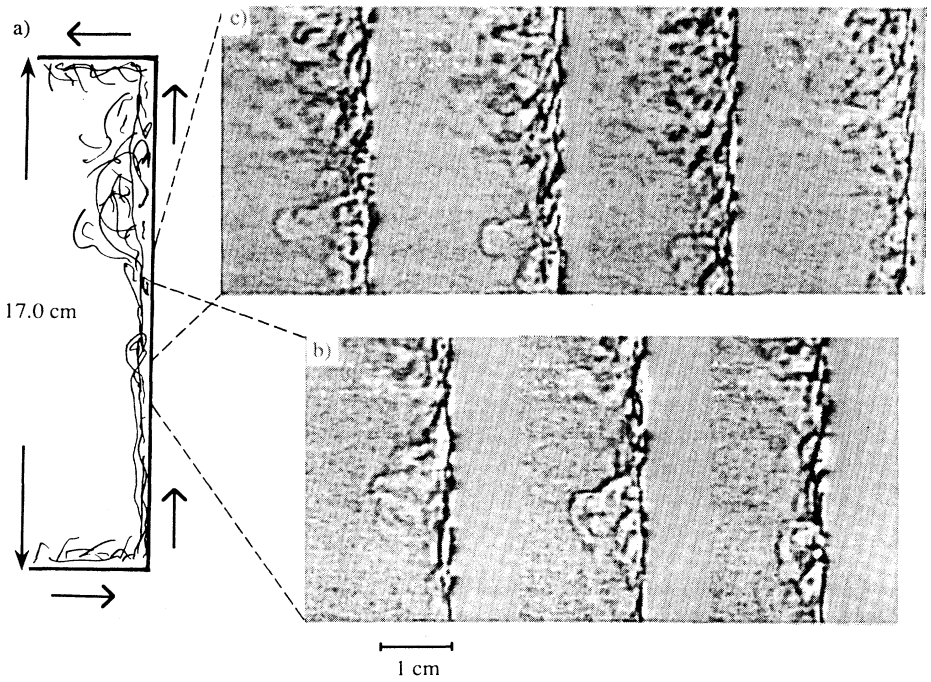

FIG. 2. (a) Sketch of the observed flow along the vertical hot plate (height $L=17$ cm). The wide arrows indicate the direction of the large scale flow. (b) Expanded image of intermittent burst, height 5.5–9.5 cm, time between frames 4/30 sec (right to left). (c) Expanded image of intermittent burst and beginning of turbulent region, height 7–11 cm, time between frames 4/30 sec (right to left).

microtranslational stage [2,6]. The movable probe in the center (7) in Fig. 1(b) was correlated with the fixed probe (3) to measure the spatial correlation of the internal waves. Thermistors in the hot and cold plates [8,9] were used to measure the temperature difference Δ between the two plates.

We start by describing the results for the turbulent states, $\mathrm{Ra} > 3\times 10^7$. Typical profiles of the mean temperature $\langle T \rangle$, the rms temperature deviation T_{rms}, and skewness are shown in Figs. 3, 4, and 5, respectively. The profiles were measured as a function of distance y from the center of the cold plate. The mean temperature shown is normalized as $(\langle T \rangle - T_{\mathrm{cold}})/\Delta$, so that it ranges from 0 at the cold plate ($y=0$) to 1.0 at the hot plate ($y=L$). The fact that this dimensionless mean is not exactly 0.5 in the bulk is an effect of the vertical temperature gradient in the cell (see below), indicating that the measurements are not made precisely at midheight in the cell. The skewness of the temperature fluctuations is negative (cold) in the boundary layer region, due to the cold perturbations. At a further distance, it becomes positive due to warm fluctuations carried by the recirculating flow of the side eddy (Fig. 5). Using the position of the maximum positive skewness to estimate the length where the vertical velocity component changes sign (eddy center), we find a distance of 7–9 mm from the wall ($0.06L$). This is to be compared to $0.09L$ found by Elder in his cell.

As in turbulent Rayleigh-Bénard convection, the imposed mean temperature gradient in our cell (which is horizontal) is confined to a small boundary layer region at

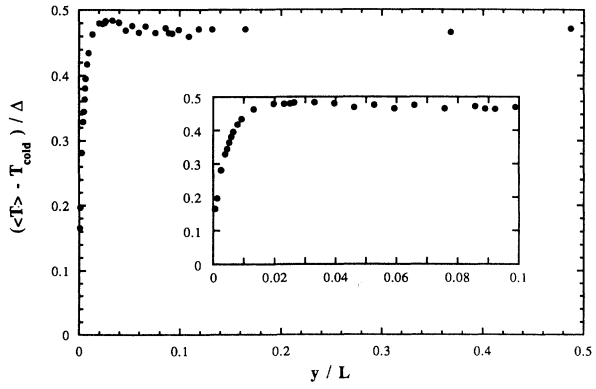

FIG. 3. At $\mathrm{Ra}=2.6\times 10^9$, the normalized mean temperature $(\langle T \rangle - T_{\mathrm{cold}})/\Delta$, as a function of distance y from the cold plate normalized by the plate separation L. The inset shows the region near the plate.

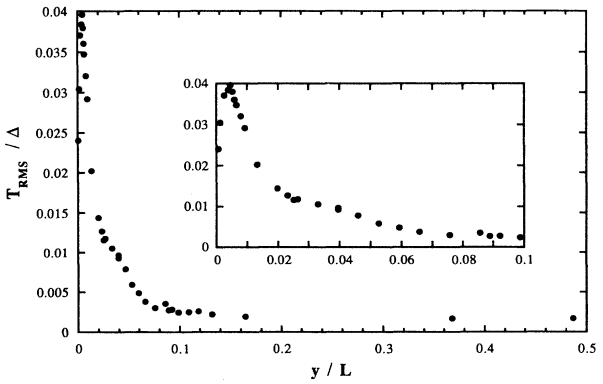

FIG. 4. At $\mathrm{Ra}=2.6\times 10^9$, the normalized rms temperature deviation T_{rms}/Δ as a function of y/L. The inset shows the region near the plate.

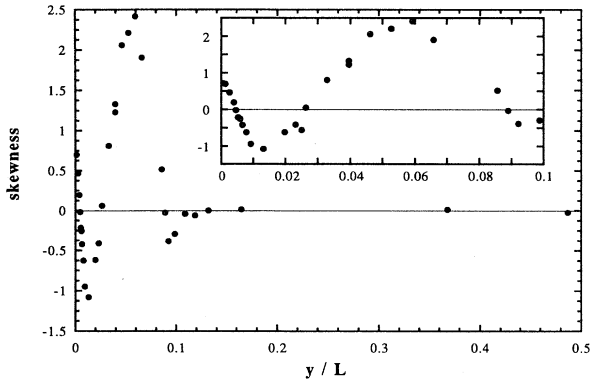

FIG. 5. At $Ra=2.6\times10^9$, the temperature skewness as a function of y/L. The inset shows the region near the plate.

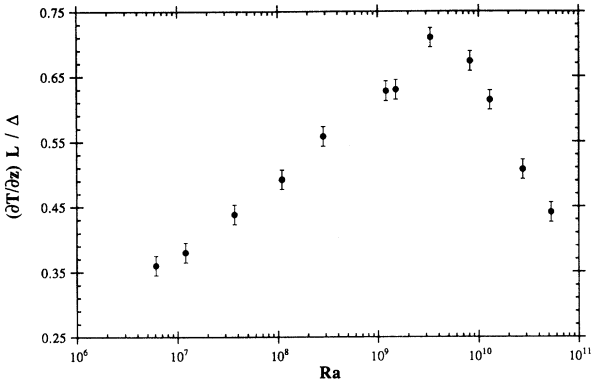

FIG. 7. The vertical gradient at the center of the cell, normalized by the imposed horizontal gradient Δ/L, vs Rayleigh number.

each isothermal plate. On the other hand, there is a vertical temperature gradient in the center (shown in Fig. 6), which exceeds the gradient in the boundary layers by 30%. The measured vertical gradient in the center of the cell is shown as a function of Ra in Fig. 7. The total vertical temperature drop (measured in a separate set of experiments with two thermistors close to the horizontal walls) is a substantial fraction of the applied horizontal temperature difference Δ, as high as 0.7Δ for $Ra\sim10^{10}$ (Fig. 7).

In Fig. 8 we show a temperature time series recorded in the center of the cell and its Fourier spectrum, indicating a nearly periodic motion: waves. The oscillation period is about 4 sec, at least an order of magnitude slower than the fluctuations near the plate. As the thermistor is moved closer to the wall, one still observes the main frequency f_0 of these waves, plus a progressively growing spectral background, which decays from a maximum at zero frequency to higher frequencies similar to spectra recorded in turbulent flows. The peak in the spectrum at f_0 cannot be discerned within 10 mm of the plate.

Since the fluid is stably stratified in the center, it is natural to interpret these oscillations as internal waves propagating in the cell. In a stably stratified fluid, buoyancy acts as a restoring force, and oscillations are possible. Neglecting thermal diffusion, viscosity, and boundary effects, assuming a linear vertical temperature dependence and small wave amplitude, the frequency of these oscillations ν is given by [9]

$$\nu=\nu_{BV}\sin\theta, \quad \nu_{BV}\equiv\sqrt{g\alpha(dT/dz)}\ , \tag{1}$$

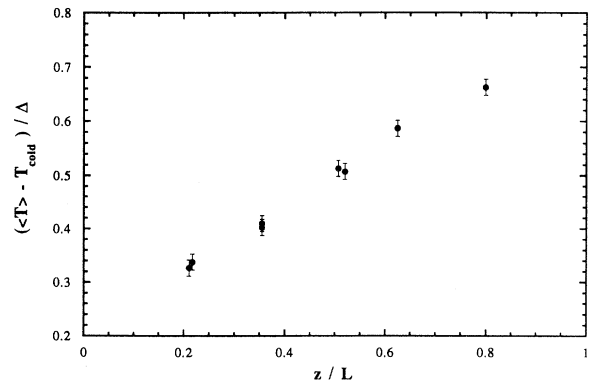

FIG. 6. At $Ra=8.2\times10^9$, the normalized mean temperature $(\langle T\rangle-T_{cold})/\Delta$ as a function of normalized height z/L, measured along the centerline of the cell.

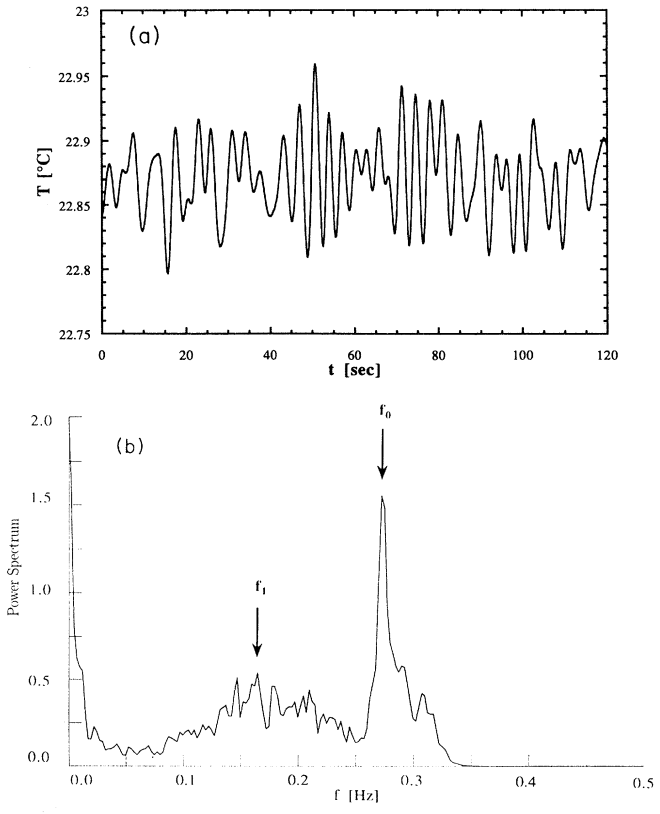

FIG. 8. Internal waves recorded in the center of the cell: (a) temperature time series, and (b) power spectrum for $Ra=3\times10^9$. In Fig. 8(b), the arrows indicate the frequencies $f_0\sim275$ mHz and $f_1\sim160$ mHz, discussed in the text; the y axis is in arbitrary units.

where θ denotes the angle of the direction of wave propagation with the vertical, g the gravitational acceleration, α the coefficient of thermal expansion, and dT/dz the vertical temperature gradient. The Brunt-Väisälä frequency ν_{BV} corresponds to waves propagating horizontally ($\theta=90°$) with vertical particle displacement. It is the highest frequency attainable for internal waves.

In Fig. 9 we compare the frequency f_0 of the peak in the spectrum with ν_{BV} calculated from the vertical temperature gradient dT/dz measured in the center. These frequencies are identical to within errors and scale as $\mathrm{Ra}^{0.6}$. Thus we conclude that the observed temperature fluctuations are due to internal waves. Using the temperature rms and the vertical gradient, we estimate a wave amplitude $A \sim 0.2$ mm (or $10^{-4}L$), independent of Ra.

Note that the frequency given by Eq. (1) does not depend on the wavelength, which is characteristic of internal waves [10]. We therefore estimate this wavelength λ experimentally. We measure the correlation C between the temperature at the center of the cell and the temperature measured simultaneously at a horizontal distance d from the center (Fig. 10). For perfectly coherent waves of wavelength δ propagating horizontally, $C(d)$ is written

$$C(d) \sim \left\langle \cos(\omega t)\cos\left[\omega t + \frac{2\pi d}{\delta}\right]\right\rangle \sim \cos\left[\frac{2\pi d}{\delta}\right], \quad (2)$$

where brackets denote a time average. Thus δ is the correlation length of the waves. The actual motion in the cell is expected to be a random superposition of finite wave trains propagating in different directions. This will make the correlation decrease faster with d than Eq. (2) would indicate, since there is no mechanism to enhance the coherence of a perfectly coherent wave. By adjusting δ, we fit the function $\cos(2\pi d/\delta)$ to the calculated correlation. From this we obtain a lower bound on the wavelength λ (i.e., $\lambda > \delta$), since if λ were less than δ, the correlation would decay faster than $\cos(2\pi d/\delta)$. A typical correlation $C(d)$ is shown in Fig. 10, together with the fitted function. The values of δ are shown in Fig. 11 as a function of Ra. For $\mathrm{Ra} < 10^9$, $\delta \sim L$, so λ must be of the order of the cell size. This motion is more accurately described as a rocking motion rather than wave propagation. For $\mathrm{Ra} > 10^9$, δ decreases with Ra, indicating either a decrease in λ, or an increasingly incoherent superposition of oscillations. For $\mathrm{Ra} > 10^{10}$, $\delta \sim 0.5L$.

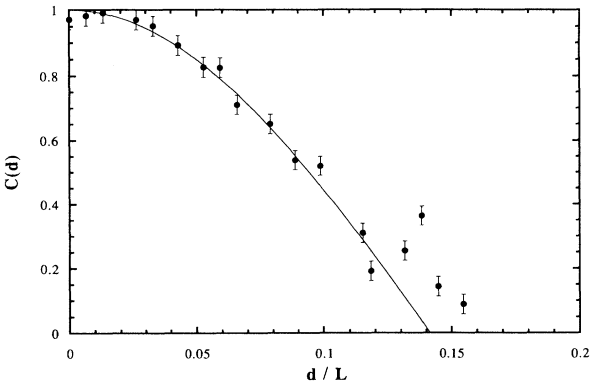

FIG. 10. The correlation $C(d)$ between the temperature signal measured in the center and at a horizontal distance d away from the center, for $\mathrm{Ra} = 8.2 \times 10^9$. The solid line is a fit to the function $\cos(2\pi d/\delta)$, where δ is defined as the correlation length.

In addition to the main frequency $f_0 \sim \nu_{BV}$, the spectrum measured in the center [Fig. 8(b)] contains a much broader peak centered at $f_1 \sim 0.7\nu_{BV}$. The position and the integrated spectral density (area under the peak in the power spectrum) at f_1, relative to the position and integrated spectral density of the peak f_0, are independent of Ra for $\mathrm{Ra} > 10^7$. In this range of Rayleigh numbers, the profiles of mean temperature, temperature rms, and skewness are also unchanged, so that the interval $3 \times 10^7 < \mathrm{Ra} < 1 \times 10^{11}$ can be classified as a single regime.

We now briefly discuss the lower Ra regimes, which we have not explored in detail. For Ra from 3×10^5 to 2×10^6, no temperature fluctuations could be detected anywhere in the cell: the flow is laminar. At $\mathrm{Ra} = 9 \times 10^6$, the spectrum near the plate consists of a fundamental frequency with 8 harmonics extending above the noise level (Fig. 12). The frequency of this mode is different from ν_{BV} (the period is about 2 sec), cor-

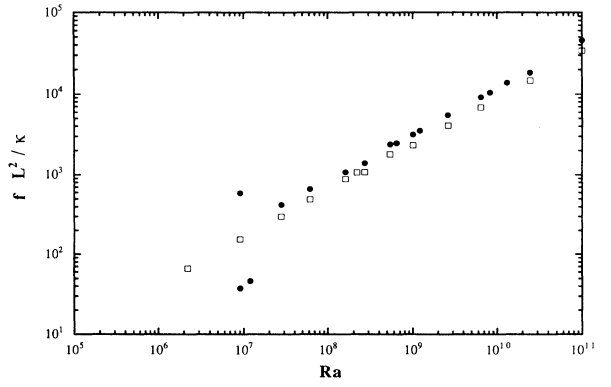

FIG. 9. The observed frequency f_0 in the spectra at the center of the cell (black dots), and the calculated Brunt-Väisälä frequency ν_{BV} based on the vertical gradient in the center (white squares), vs Rayleigh number. The frequencies are made dimensionless by the characteristic time L^2/κ.

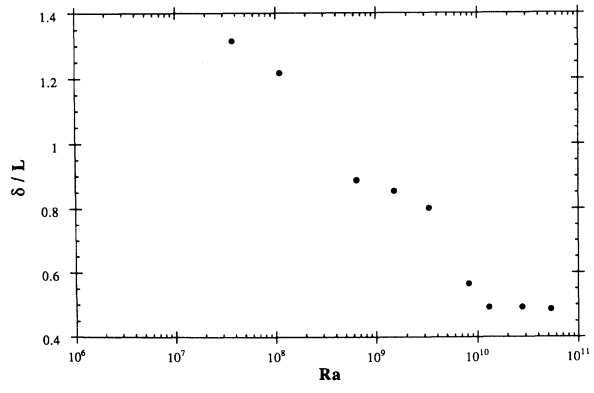

FIG. 11. The normalized correlation length δ as a function of Rayleigh number.

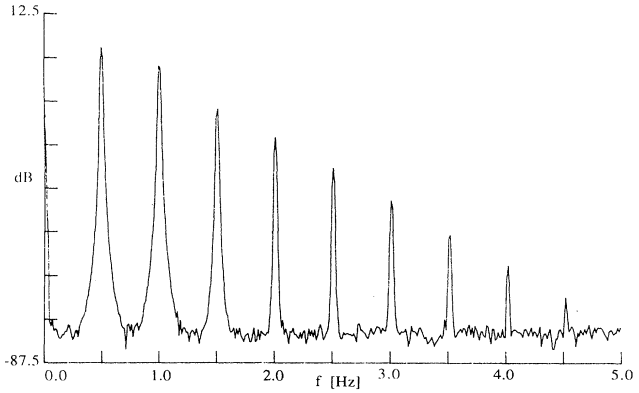

FIG. 12. At $Ra=9.0\times10^6$, the power spectrum of the temperature time series recorded 6.0 mm from the center of the cold plate; the y axis is in arbitrary units. The main frequency is about 0.5 Hz, followed by 8 harmonics.

responding to a different type of motion, which will not be discussed in this paper.

Finally, Fig. 13 shows the thickness of the thermal boundary layer (defined as the position at which the temperature rms is maximum, as discussed in [11]) as a function of Ra. In the range of Ra from 5×10^5 to 1×10^{11}, the scaling of the boundary layer with Ra has an exponent 0.29. This exponent value is identical to the one measured in the upright Rayleigh-Bénard cell [1,2]. The prefactor in the Rayleigh-Bénard cell is larger by 12%.

V. DISCUSSION

We now start the discussion of the results by relating the flow field to the profile of mean and rms temperatures. We recall that the recirculating flow of the side eddies is at a distance of 7–9 mm from the sidewalls. At the top of the cold sidewall, warm fluid is deflected downwards. In the vicinity of the wall, heat transport is purely diffusive and a strong temperature gradient develops. Further away from the wall, the warm fluid is not thermalized by the time it reaches the thermistor, and a

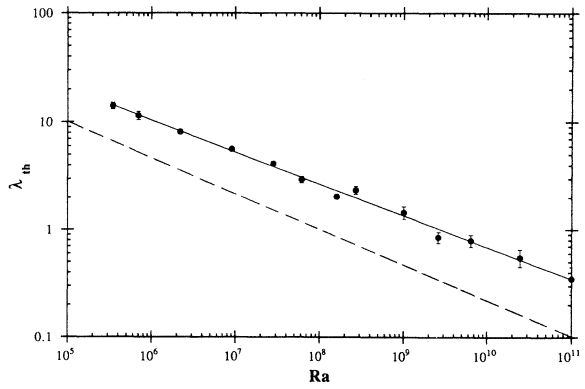

FIG. 13. The thickness of the thermal boundary layer, as defined in the text, vs Ra. The line through the points corresponds to $Ra^{-0.29}$; the dashed line corresponds to $Ra^{-1/3}$.

dimensionless mean temperature $(\langle T\rangle - T_{cold})/\Delta$ in excess of 0.5 is expected. An overshoot is indeed observed at a distance of 4 mm ($y/L\sim0.025$) for $Ra=2.6\times10^9$, as shown in Fig. 3. Further from the wall, the region of closed streamlines of the side eddies is entered, in which fluid from the center is carried around in loops, so that thermalized fluid is already found at distances less than 8 mm. Similarly, the rms profile has a maximum at the edge of the thermal boundary layer, where both a large mean temperature gradient and appreciable velocity fluctuations exist. The temperature rms then decays for distances larger than 0.8 mm ($y/L\sim0.005$) for $Ra=2.6\times10^9$. A second, much weaker peak is observed, see Fig. 4, in the region from about 4 to 8 mm (y/L around 0.04). One can relate it to the mixing of thermalized gas from the center (entrained by the side eddy) with still warm gas carried by the large scale circulation.

The presence of a stabilizing vertical temperature gradient is easily understood: the large scale circulation carries hot gas to the top and cold gas to the bottom of the cell. The fast moving flow at the perimeter of the cell is unstable and better mixed than the quiescent gas in the center, so that a stronger vertical gradient survives in the center of the cell. The more turbulent flow of the large scale circulation along the plates destroys this stabilizing gradient in the neighborhood of the walls.

In Fig. 7, a maximum in the vertical gradient measured at the center occurs around $Ra=3\times10^9$. Based on our experiment, we are unable to say if this is an actual maximum in the gradient, or the result of the finite spacing of our temperature probes used to measure it. A more thorough investigation of the vertical temperature profile in this system is warranted.

We next turn our attention to the waves in the central region of the cell. Figure 8(a) typifies the situation: random trains of gravitational waves driven by the turbulent fluctuations at the boundary layers. We have presented our observations in the framework of linearly superposed waves, neglecting diffusivities (thermal and momentum) and boundary effects. The ratio of wave amplitude to wavelength is indeed so small that no wave breaking or nonlinear interaction is expected. The oscillation period is shorter than the thermal diffusion times scale (wavelength squared over diffusivity) by at least an order of magnitude, so that neglectng the diffusivities is justified. However, the waves are propagating in a medium with a nonuniform vertical temperature gradient and bounded by shear flows; furthermore, the wavelength is comparable to the cell size. A more accurate analysis should include the boundaries and the turbulent flow, as discussed for example in [12]. Nonetheless, the main peak in the spectrum is clearly due to internal waves excited by disturbances and fluctuations in the large scale circulation. The estimated wavelength δ decreases with Ra, which could be due to the large scale circulation becoming turbulent and producing a less coherent superposition of wave trains at higher Ra. Also, the length scale of the turbulent structures at the boundaries is decreasing with Ra, which could excite waves of smaller wavelength.

A more puzzling feature of the spectrum in Fig. 8(b) is the broad range of wave frequencies around $f_1\sim160$

mHz, occurring below the Brunt-Väisälä peak at $f_0 \sim 275$ mHz. These lower frequencies may correspond to internal waves propagating in a direction around 36° from the vertical, using f_1 in Eq. (1). Such waves would thus propagate approximately from corner to corner of the cell, excited by the fluctuations there, where the flow has to take a narrow curve. The corners are an interesting and ill-understood region of the side-heated convection cell, for they are also where the large scale flow feeds into the side eddies near the plates. Another possible candidate for an excitation mechanism of the lower frequencies is a parametric instability of the type demonstrated in [13].

We finally compare the flow studied in this paper with the hard turbulent state of Rayleigh-Bénard convection [1,2,14]. Both flows show a large scale circulation, which occurs naturally in the side-heated case but implies symmetry breaking in the Rayleigh-Bénard case. A surprising difference is the occurrence of the two recirculating side eddies in side-heated convection; we know of no explanation for this phenomenon. Side-heated convection is considerably less disordered than Rayleigh-Bénard convection, in that the flow is only chaotic or even laminar for Rayleigh numbers at which Rayleigh-Bénard convection is already turbulent. This is strong evidence of the relaminarizing effect of the stable stratification which characterizes the bulk of the side-heated cell.

Turbulent flows are to a large degree controlled by the activity at the boundary. In the Rayleigh-Bénard geometry, pieces of thermal boundary layer driven by buoyancy may separate from the plates and form plumes, coupling the bulk of the cell to the boundary layer. In the side-heated geometry, boundary layer detachments simply travel along the sidewall leaving the bulk largely undisturbed. The side eddies may further protect the center from boundary layer instabilities. Although the stable stratification suppresses motion in the center, making it a much more quiet environment than in the Rayleigh-Bénard case, the boundary layer fluctuations still couple to the bulk enough to drive the waves; the side-heated cell is divided into an almost stationary bulk and a turbulent perimeter. The thermal stratification in the bulk sets a frequency scale, which corresponds to the oscillations of internal waves. In Rayleigh-Bénard convection, a characteristic frequency appearing in the spectra which scales as $\mathrm{Ra}^{0.5}$ was identified as the inverse turnover time of the large scale circulation [14]. The Brunt-Väisälä frequency here scales as $\nu_{\mathrm{BV}} \sim \mathrm{Ra}^{0.6}$.

In view of all the differences, it is all the more surprising in comparing the two experiments that the thermal boundary layer thickness scales with the same exponent, and with only a slightly different prefactor. The boundary layer thickness determines the Nusselt number. The present measurements determine the boundary layer thickness at only one location, whereas the total Nusselt number is determined by the spatially averaged thickness. The scaling law should however be the same for the average and local thickness [2,6], so that the Nusselt number can be expected to scale as $\mathrm{Ra}^{2/7}$ in both geometries. This power law observed in Rayleigh-Bénard convection constitutes one of the distinguishing marks of the "hard turbulence" regime, and has so far defied any undisputed theoretical explanation. The fact that this scaling occurs in two drastically different flows suggests that a simple mechanism underlies the dependence of the Nusselt on the Rayleigh number; $\frac{2}{7}$ is robust.

[1] X. Z. Wu and A. Libchaber, Phys. Rev. A **45**, 842 (1992).
[2] A. Belmonte, A. Tilgner, and A. Libchaber, Phys. Rev. E **50**, 269 (1994).
[3] E. R. G. Eckert and W. O. Carlson, Int. J. Heat Mass Transfer **2**, 106 (1961); N. Seki, S. Fukusako, and H. Inaba, J. Fluid Mech. **84**, 695 (1978); Y. Lee and S. Korpela, *ibid.* **126**, 91 (1983).
[4] J. W. Elder, J. Fluid, Mech. **23**, 77 (1965).
[5] J. W. Elder, J. Fluid Mech. **23**, 99 (1965).
[6] A. Belmonte, Ph.D. thesis, Princeton University, 1994 (unpublished).
[7] W. Merzkirch, *Flow Visualization* (Academic, New York 1987).
[8] The video card used in a PixelPipeline card (Perceptics Corp., Knoxville, TN). The programs used are NIH Image 1.49 VDM (National Institute of Health, Washington D.C.), and IPLab (Signal Analytics Corp., Vienna, VA).
[9] V. Väisälä, Soc. Fennica Commun. Math. Phys. **2**, 38 (1925); D. Brunt, Q. J. R. Meteorol. Soc. **53**, 30 (1927); M. E. McIntyre, in *Atmospheric Dynamics: Some Fundamentals, with Observational Implications,* Proceedings of the International School of Physics "Enrico Fermi," Course CXV, Varenna, 1990, edited by J. C. Gille (North-Holland, Amsterdam 1992).
[10] D. J. Tritton, *Physical Fluid Dynamics,* 2nd ed. (Clarendon, Oxford, 1988), pp. 208–214.
[11] A. Belmonte, A. Tilgner, and A. Libchaber, Phys. Rev. Lett. **70**, 4067 (1993).
[12] S. A. Thorpe, Philos. Trans. R. Soc. London, Ser. A **263**, 563 (1968).
[13] A. D. McEwan and R. M. Robinson, J. Fluid Mech. **67**, 667 (1975).
[14] B. Castaing, G. Gunaratne, F. Heslot, L. Kadanoff, A. Libchaber, S. Thomae, X. Z. Wu, S. Zaleski, and G. Zanetti, J. Fluid Mech. **204**, 1 (1989).

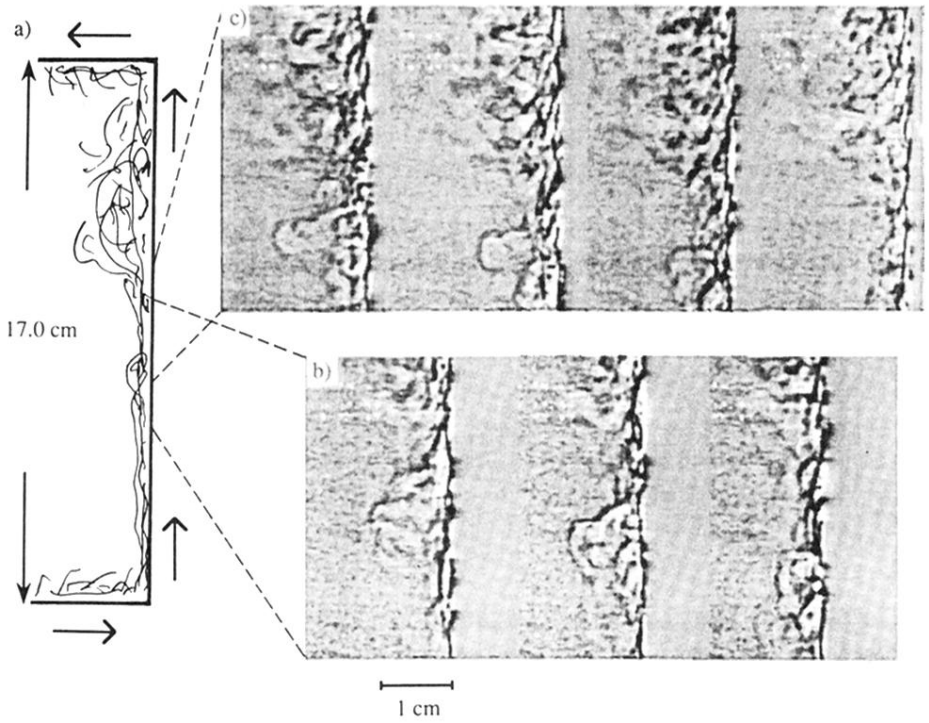

FIG. 2. (a) Sketch of the observed flow along the vertical hot plate (height $L = 17$ cm). The wide arrows indicate the direction of the large scale flow. (b) Expanded image of intermittent burst, height 5.5–9.5 cm, time between frames 4/30 sec (right to left). (c) Expanded image of intermittent burst and beginning of turbulent region, height 7–11 cm, time between frames 4/30 sec (right to left).